

The Sun as a star: observations of white-light flares

Matthieu Kretzschmar

▶ **To cite this version:**

Matthieu Kretzschmar. The Sun as a star: observations of white-light flares. Astronomy and Astrophysics - A&A, 2011, 530, A84 (7 p.). 10.1051/0004-6361/201015930 . insu-01253673

HAL Id: insu-01253673
https://insu.hal.science/insu-01253673

Submitted on 11 Jan 2016

HAL is a multi-disciplinary open access archive for the deposit and dissemination of scientific research documents, whether they are published or not. The documents may come from teaching and research institutions in France or abroad, or from public or private research centers.

L'archive ouverte pluridisciplinaire **HAL**, est destinée au dépôt et à la diffusion de documents scientifiques de niveau recherche, publiés ou non, émanant des établissements d'enseignement et de recherche français ou étrangers, des laboratoires publics ou privés.



Distributed under a Creative Commons Attribution - NonCommercial - NoDerivatives 4.0 International License

A&A 530, A84 (2011)
DOI: 10.1051/0004-6361/201015930
© ESO 2011

Astronomy & Astrophysics

The Sun as a star: observations of white-light flares

M. Kretzschmar

LPC2E, UMR 6115 CNRS and University of Orléans, 3a Av. de la recherche scientifique, 45071 Orléans, France
e-mail: matthieu.kretzschmar@cnrs-orleans.fr

Received 14 October 2010 / Accepted 1 April 2011

ABSTRACT

Context. Solar flares radiate energy at all wavelengths, but the spectral distribution of this energy is still poorly known. White-light continuum emission is sometimes observed, and these flares are then called "white-light flares" (WLFs).
Aims. We investigate if all flares are WLFs and how the radiated energy is distributed spectrally.
Methods. We perform a superposed epoch analysis of spectral and total irradiance measurements obtained since 1996 by the SOHO and GOES spacecraft at various wavelengths, from soft X-rays to the visible domain.
Results. The long-term record of solar irradiance and the excellent duty cycle of the measurements allow us to detect a signal in visible irradiance even for moderate (C-class) flares mainly during the impulsive phase. We identify this signal as continuum emission emitted by WLFs and find that it is consistent with a blackbody emission at ~9000 K. We estimate the contribution of the WL continuum for several sets of flares and find it to be about 70% of the total radiated energy. We re-analyse the X17 flare that occurred on 28 October 2003 and find similar results.
Conclusions. We show that most of the flares – if not all – are WLFs and that the white-light continuum is the main contributor to the total radiated energy; this continuum is consistent with a blackbody spectrum at ~9000 K. These observational results are important for understanding the physical mechanisms during flares and possibly suggest a contribution of flares to the variations of the total solar irradiance (TSI).

Key words. sun: flares – stars: flare – Sun: activity – solar-terrestrial relations

1. Introduction

Solar flares are huge bursts of energy in the atmosphere of the Sun. Satellite observations have were increased in the extreme ultraviolet (EUV) and soft X-ray (SXR) domain, which was not possible before the space age. At these wavelengths, the emission increases drastically and can last for a few hours (depending on the flare magnitude). Flares were first observed from the ground in the visible domain (Carrington 1859; Švestka 1966; Neidig 1989), however, and the advent of spectroscopic observations revealed the increase of solar flux in visible spectral lines, sometimes changing from absorption to an emission profile (Hale 1931; Schmieder et al. 1998).

Flare emission in the visible domain is thus well known to occur in visible chromospheric lines like the Balmer and Ca II K lines (Canfield et al. 1990; Falchi et al. 1992; Heinzel et al. 1994). There is, however, another – and less well understood – contribution to the visible emission that is due to the enhancement of the continuum. The term "white-light" (WL) is used to refer to visible continuum enhancement. The study of WL flares has been rendered very difficult by their short duration and very low contrast, which makes their observations from Earth rare and of poor quality. Neidig (1989) emphasized this aspect and suggested that WL emission can be quite common and can constitute up to 90% of the total energy radiated by the flare. This has, however, never been confirmed and several questions remain about WL emission, such as: what is the contribution of WL emission to the total flare energy? Does it appear only in very large flares? How and where is it produced?

There are only a few observations of WLFs in space because the available measurements do not in general have the required high spatial and temporal resolution or the necessary duty cycle. Several WLFs have, however, been observed with Yohkoh (e.g. Matthews et al. 2003) and TRACE (e.g. Hudson et al. 2006); these studies have confirmed the importance of WLFs and their association with the hard X-rays in the impulsive phase of the flare. Furthermore, many flares were observed with no associated white-light emission and with no means to determine if this was because of instrumental limitations or because of the actual absence of WL emission. Recent studies (Jess et al. 2008; Wang 2009) identified WL emission in relatively small flares, which supports the view that WL emission could be a peculiar feature of a flare and not associated to the largest flares only.

Knowing how much energy is radiated as a whole and at each wavelength is important both to understand the physical processes in the solar atmosphere and the impact of flares on Earth. Ideally, it would be necessary to observe the Sun at all wavelengths with sufficient contrast (implying good spatial and temporal resolution) and duty cycle (to avoid missing the flare). One must often deal with partial observations only, especially at ultraviolet and visible light where contrast is weak and space instrumentation is rare. This explains why we still have a partial view of how the flare energy is spectrally distributed. Woods et al. (2004, 2006) provided the first direct observation of a flare signal in the total solar irradiance (TSI), thus allowing a precise estimate of the the total energy radiated by the extremely large (X17) flare of October 28, 2003. Using additional solar irradiance observations in the XUV (shorter than 27 nm) and the FISM flare model up to 190 nm, Woods and collaborators concluded that about half of the energy is radiated below 190 nm, most of it coming from wavelengths shorter than 14 nm and the other half coming from near UV, visible, and infrared light. These

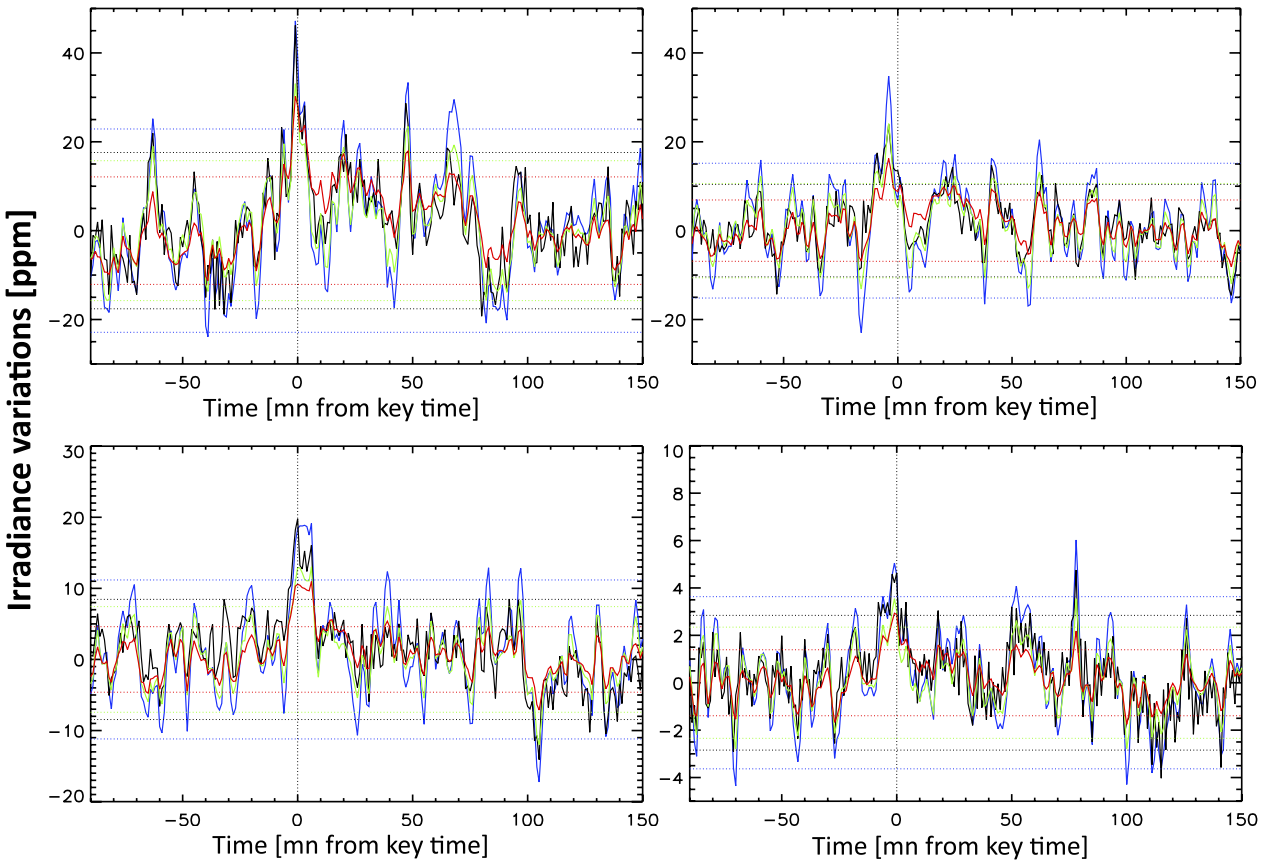


Fig. 1. Average flare light curves for TSI (black), and the three visible SPM channels (blue, green, and red). *Upper left panel*: average over 43 flares from X17.2 to X1.3. *Upper right panel*: average over 68 flares from X1.3 to M6.4. *Lower left panel*: average over 140 flares from M6.4 to M2.8. *Lower right panel*: average over 1850 flares from M2.8 to C4. Horizontal lines show the $\pm 2\sigma$ limits computed from –90 to 150 min excluding 60 min centred around the peak time.

important results for very large flares suffer from the absence of direct observations at wavelengths longer than 27 nm and assume that the TSI time profile follows the flare time profile in XUV. In this paper we show that white-light continuum is commonly produced in basically all flares and that it represents most of the flare energy. In Sect. 2 we present the data and the analysis method. We follow Kretzschmar et al. (2010) and perform a superposed epoch analysis of solar *irradiance* (i.e., integrated solar flux) in the visible domain during flares. The exceptional duty cycle and long-term monitoring of the Sun PhotoMeter (SPM) instrument counterbalance the absence of spatial resolution and the presence of background temporal fluctuations from p-modes and granulation, which allows us to reveal the flare signal at visible wavelengths and to identify it as WL continuum (Sect. 3). In Sect. 4 we estimate the spectral distribution of the radiated energy for average flares of different amplitude as well as for the single X17 flare of October 28, 2003, for which we present new observations. We conclude in Sect. 5.

2. Data and analysis

The data we used are full Sun fluxes (i.e. solar irradiance) observed by the SOHO and GOES spacecraft: the TSI (solar flux integrated over all wavelengths), measured by the VIRGO/PMOv6 instrument onboard SOHO; three *Visible Solar Irradiance* from the VIRGO/SPM instrument (still SOHO) consisting of three passbands of 5 nm centred on 402 nm (blue), 500 nm (green), and 862 nm (red) respectively. These irradiance time series cover the period from 1996 to mid 2008 with a 1-min time step with very few data gaps. They have been corrected for degradations and can be downloaded from the VIRGO ftp website[1]. Additionally we use the EUV irradiance in the ranges 0.1–50 nm and 26–34 nm measured by SOHO/SEM (Judge et al. 1998) and the SXR irradiance measured by the GOES satellites.

The superposed epoch analysis is relatively simple and consists in superposing several time series in which a similar event (here a flare) occurs at the same time. It is useful when the signal of the event is faint with respect to the random (incoherent) background fluctuations. The resulting superposed (or average) curve thus exhibits lower background fluctuation (typically attenuated by a factor $1/\sqrt{n}$, n being the number of samples) but a stronger signal at the time of the event, which results from the superposition of all coherent faint signals in each individual time series. This technique has been used to detect flares in TSI and in the disk integrated Na D line (Kretzschmar et al. 2010; Cessateur et al. 2010); we extend these studies here by looking at visible, EUV, and SXR irradiance time series.

The events we consider here are flares observed in SXR by the GOES satellites from 1996 to 2007, which occured at heliocentric angle $\theta \leq 60$ deg because at higher θ the visible emission is likely to be strongly absorbed. Before superposing the light curves for the TSI and visible irradiance, we subtracted a linear fit from the time series to eliminate trends. This could

[1] ftp.pmodwrc.ch/pub/data/irradiance/virgo/1-minute_Data/

in principle hide meaningful trends (for example linked to the evolution of the active region pre- or post- flare) but it allows us to reach a better signal-to-noise ratio, and the analysis without trend removal did not reveal clear results. In Sect. 4 we analyse the spectral distribution of the flare energy; for this purpose, we converted the TSI and visible light curves from ppm to irradiance units (W m^{-2}) by simply multiplying the average time series by their average value (1365 W m^{-2}, for the TSI, 1.67 W m^{-2}, 1.83 W m^{-2}, 0.97 W m^{-2} for the blue, green, and red channel respectively); small departures from theses values (for example by taking 1361 W m^{-2} instead of 1365 W m^{-2} for the TSI) do not affect the result because of the difference of many orders of magnitude between the quiet irradiance and the flare flux. The averaged light curves in physical units for the EUV and SXRs channels are obtained by subtracting the background of each time series before averaging.

3. White-light flare observations in Sun-as-a-star measurements

Figure 1 shows the average flare light curves for four sets of flares of decreasing magnitude in the visible and TSI channels. The GOES SXR peak time was chosen as the key time for each flare. The first immediate result is the appearance of a peak in all channels around the key time that is caused by the flares. Importantly, this is true down to C-class flare, although it can be noted that the signal-to-noise ratio is lower. This shows in particular that visible emission is ubiquitous in flares. We can note that other peaks exceed the 2σ limits (about 5 points over 100, as expected for random noise); they are less pronounced, however, and appear at different times for the different flare sets. The curves also display oscillations with roughly a 10 to 20-min period, whose amplitude is below the 2σ level (see also Fig. 4 before peak time); it is not clear whether these oscillations can be related to actual solar processes (pre- and post- flare accoustic waves) or if they are artefacts of the instrumental noise. The fact that they are not in phase for different flare sets rather points towards an instrumental effect.

The curves exhibit several additional interesting features. First, most of the visible emission belongs to the impulsive phase of the flare. This can be better seen in Fig. 2; when the key time is the GOES SXR peak time, the maximum of the curves precedes it, while when the key time is the peak of the derivative of the SXR flux, the maximum occurs at $t = 0$. The amplitude of the increase is larger when using the SXR flux peak; we attribute this to the fact that the Neupert effect does not hold rigorously in all flares. Figure 3 shows in a similar way the effect of the duration of the impulsive phase, computed as the duration of the rising phase of the SXR flare, i.e. $t_{\rm SXR}^{\rm peak} - t_{\rm SXR}^{\rm start}$. The flare signal in the visible channels and in the TSI nearly disappears after the SXR peak time for flares with a short impulsive phase (≤6 min), while it persists for flares with a longer impulsive phase (>6 min). This suggests that visible emission is present in both compact and gradual flares, but that it also persists for some time during the gradual phase of gradual flares.

The second point to note in Fig. 1 is the longer decay of the red channel after the peak, which can be attributed to the chromospheric Ca II line emission that is included in this channel. This constitutes a clear signature of the gradual phase, which is not seen in the blue and green channel, and is much less obvious in the TSI measurements.

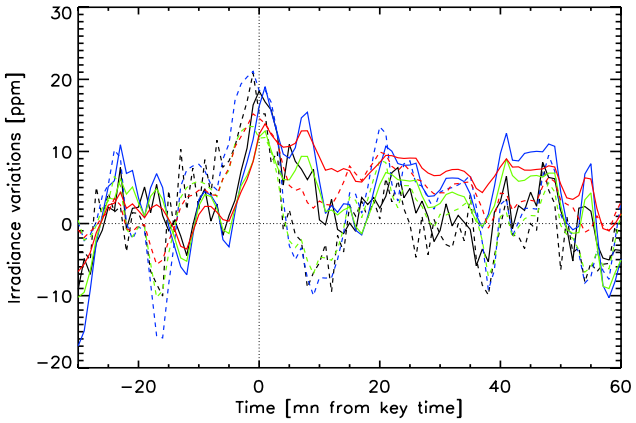


Fig. 2. Influence of the key time on the analysis. Dashed lines are average flare time series using the GOES 0.1–0.8 nm flux peak time, thick lines are average flare time series using the peak time of the derivative of the GOES 0.1–0.8 nm flux. Black is for TSI, red for 862 nm, blue for 402 nm, and green for 500 nm. The average is made over the 150 largest flares in our sample, from X28 to M5.

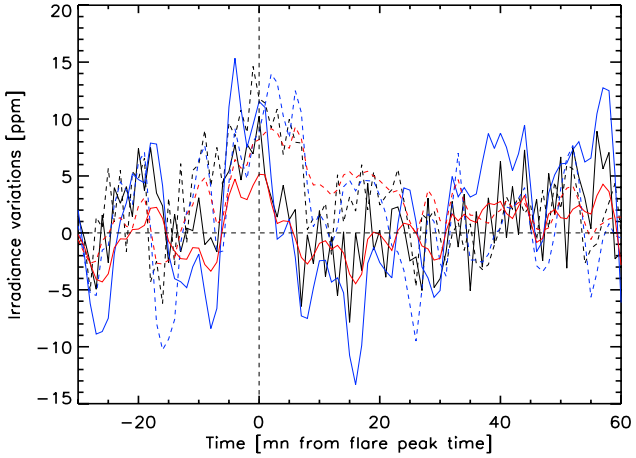


Fig. 3. Influence of the impulsive phase duration on the analysis. Thick lines show average time series for flares with short impulsive phase (equivalent X-ray class M2), dashed lines for long impulsive phase (equivalent X-ray class M5). SPM green is not shown for clarity but behaves similarly to SPM blue.

Thirdly, the flare emission in the blue tends to be higher than in the two other visible channels. We come back to this point below, but let us note now that it agrees with the general statement that stellar flares are "blue", i.e., display more emission towards the UV (e.g. Hawley et al. 2003).

Last, but not least, the relative increase in the visible channels is nearly of the same amplitude as for the TSI. This strongly suggests that the visible emission has a dominant contribution in the total energy radiated by flares. We also come back to this point below.

Figure 1 shows that the SPM visible emission is observed on average in all flares down to C-class ones. Does this emission come from lines or from the continuum? The SPM channels have been chosen to be in the continuum of the solar spectrum, and their response functions computed for the quiet Sun (Jiménez et al. 2005) show that the the blue and green channel corresponds to the deep photosphere (near $\tau_{500} = 1$), while the red channel has a larger contribution from the chromosphere (the Ca II line). Yet, because a multitude of lines are present all over the optical solar spectrum, we looked at the modelled spectrum from Chance & Kurucz (2010), the observed spectrum

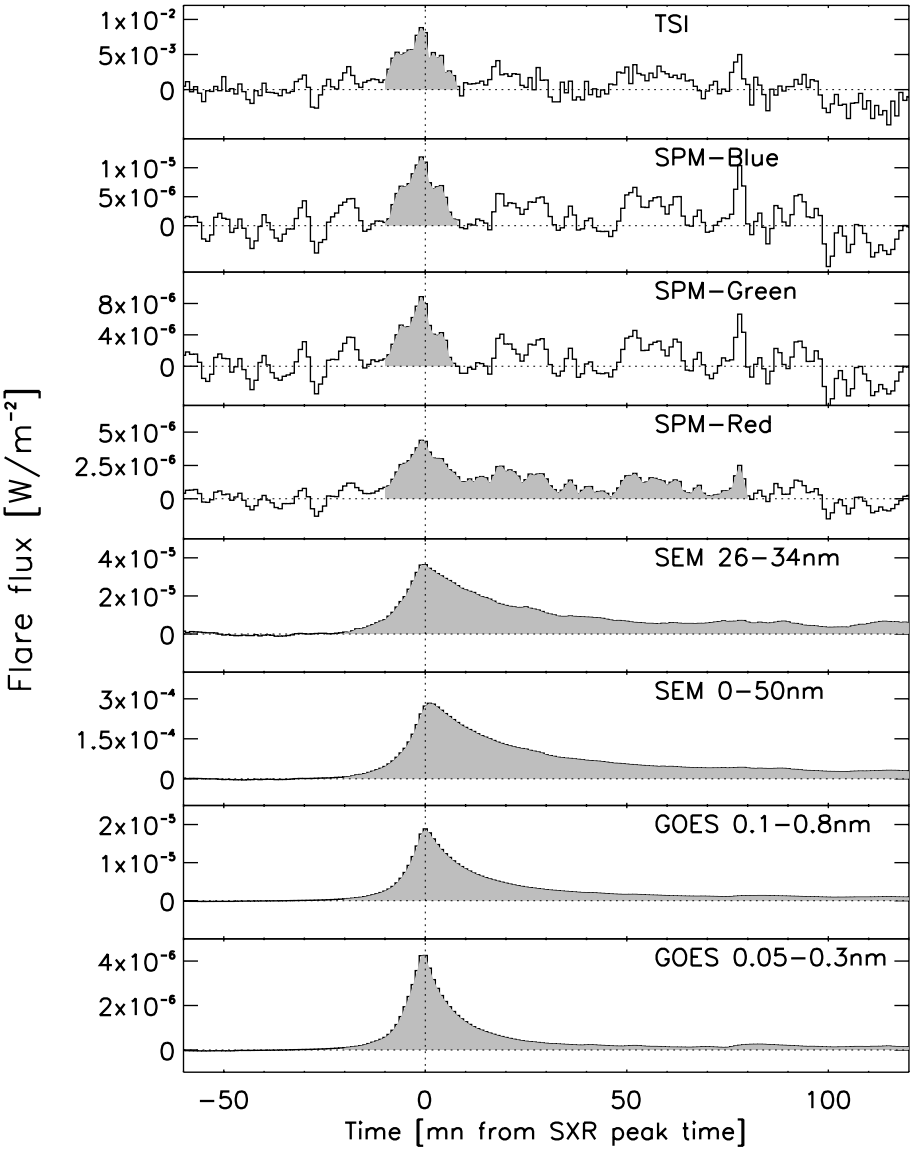


Fig. 4. Flare light curves averaged over 2100 flares (from X17.2 to C4) in various spectral ranges.

by Thuillier et al. (2004), and the observed identified line lists by Allende Prieto & Garcia Lopez (1998). The blue and green channels include only a few weak lines from neutrals (mainly Fe I), which strongly suggests that the increase of emission, observed during the impulsive phase, is caused by a general increase of the continuum level. The next section shows that this continuum is furthermore consistent with a blackbody spectrum at $T \sim 9000$ K, which agrees with solar and stellar observations of WLFs. Because we access only light curves averaged over several flares, we can wonder how often this WL continuum emission does actually occur. To test this, we substituted in our sample some of the time series that include flares with time series that do not include them (randomly selected at a time where no flares occur). The flare signal for the less energetic flare set (bottom right panel in Fig. 1) becomes visible when only one out of five time series is replaced. This roughly indicates that at least 80% of the flares have WL continuum emission and can thus be considered to be WLFs.

4. Spectral distribution of flare energy

Figure 4 shows flare light curves in several spectral bands from SXRs to visible and averaged over 2100 flares ranging from X-class to C-class. The EUV and SXR bands show a long gradual phase that can also be seen in the visible red channel that contains a chromospheric contribution. The TSI light curve should also exhibit the gradual phase that occurs at all chromospheric and coronal wavelengths, but it does not. The most probable explanation is that the gradual phase is below the noise level, which emphasizes the predominance of the impulsive phase. Because of this, we cannot exclude that the blue and green channels also have a gradual phase, although smaller than the red channel. We use Fig. 4 to estimate the spectral distribution of the flare energy and we repeat this for the four sets of flares shown in Fig. 1. Because the gradual phase is hardly observed in the TSI average light curves, we computed the energy radiated in each passband both over the total duration of the flares, i.e., including the long gradual phase when it is present, and over the restricted time for which the flare signal is seen in the TSI. For the visible irradiance and the TSI (EUV and SXR channels respectively) we limit the start of the flare integration to 10 min (20 min respectively) before the key time, to avoid signals potentially caused by background fluctuations in the visible and TSI light curves. Emission excess observed at Earth can be converted into energy release on the Sun with the factor $d_{\rm AU}^2 \times f$, where f takes into account the angular distribution of the emission. We use the following

Table 1. Spectral distribution of flare energy.

Mean X-ray class	Total energy TSI (ergs)	Ratio 26–34 nm/TSI	Ratio 0–50 nm/TSI	Ratio 0.1–0.8 nm/TSI	T_{bb} (°K)	S_f (arcsec^2)	Ratio Continuum/TSI
X3.2	5.9×10^{31}	0.9%–0.8%	12%–9%	1.2%–1%	9345	16.7	67%
M9.1	1.6×10^{31}	1.7%–0.4 %	23%–5%	1.0%–0.4%	8993	13.2	85%
M4.2	1.3×10^{31}	2.2%–0.5%	18%–6%	0.6%–0.3%	9244	7.3	74%
C8.7	3.6×10^{30}	1.5%–0.5%	16%–5%	0.4%–0.2%	8655	2.4	72%
M2.0	5.1×10^{30}	1.7%–0.6%	18%–6%	0.7%–0.4%	8941 K	2.8	69%

Notes. Spectral energy distribution. From first row to last the average corresponds to the five sets of flares shown in Figs. 1 and 4. The two ratios in Cols. 3 to 5 correspond to integrations over the entire flare duration and integrations limited to the TSI flare signal period. The three last columns show mean blackbody and flare parameters that can explain the visible emission at the flare peak time.

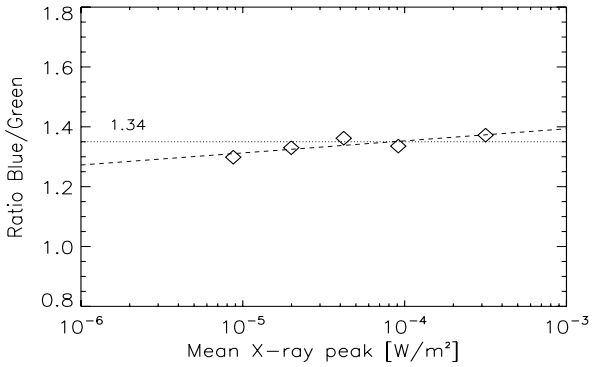


Fig. 5. Ratio between the flare maximum emission in the blue and green channel versus the mean SXR flux peak. Dotted line is the average ratio of 1.34 and the dashed line is the best fit obtained with the expression $I^f_{Blue}/I^f_{Green} = 0.04 \times \log(E_{SXR}) + 1.51$. The mean ratio can be reproduced by assuming that the flare emission follows a blackbody curve at ~9100 K.

factors: $f = 2\pi$ for optically thin emission (0–50 nm and 0.1–0.8 nm), and $f = 1.4\pi$ for the TSI and 26–34 nm channel, as suggested by Woods et al. (2006). Note that if we assume that the angular distribution is the same for all channels, the optically thin contributions are decreased by a factor 1.43. The resulting flare energy distribution is shown in Table 1 for the two integrations (next section explains the three last columns); it reveals that the short wavelength passbands are a minor contributor to the total energy, even when the gradual phase is not taken into account only for the TSI. The GOES SXR energy is less than 1% of the total energy, while all wavelengths below 50 nm represent between 10% and 20%. The visible and near UV part of the flare spectrum must thus constitute the bulk of the flare energy.

4.1. Energy in the white light continuum

It is difficult to reproduce the exact shape of the continuum spectrum from the observations of only three passbands. However, we can make simple considerations and try to estimate the total energy that goes in the continuum. White-light flares are usually divided into two types according to whether or not the emission exhibits a jump at the Balmer and Paschen edges; in our case, the blue and green passbands are just above the Balmer edge and the red channel is just above the Paschen edge; we assume in the following that the hydrogen free-bound emission contributes a negligible amount to the green and blue passbands (although the contribution of the Paschen continuum could be significant). Figure 5 shows the ratio of the flare emission in the blue and green channel I_{blue}/I_{green} at peak time; this ratio is about 1.34 and changes slowly for different flare amplitudes. We can easily convert the ratio values into blackbody temperature; a linear extrapolation of the observed increasing ratio with flare amplitude leads to temperatures ranging from $T \sim 8430$ K for C1 flares to $T \sim 9560$ K for X10 flares. The slow change in temperature with the SXR flare magnitude indicates that the spectrum shape is similar for different flare magnitudes, the amplitude of the WL continuum depending mainly on the flaring area. Table 1 gives the exact temperature found for each set of flares. These blackbody temperatures agree well with what was found previously. Hawley et al. (2003) explained the continuum emission of a flare observed on the M dwarf AD Leo with a blackbody temperature near 10 000 K; Fletcher et al. (2007) found a very upper limit of 2.5×10^4 K to reproduce the spectral ratio between UV and visible emission in several solar WL flares, while recently Kowalski et al. (2010) have provided evidence that the flare emission observed on a dMe4.5e star is composed of a Balmer component at wavelengths shorter than ~380 nm and of a $T \sim 10^4$ K blackbody component above 400 nm. White-light continuum emission is thought to occur in the minimum temperature region or below, where heating is provided by radiative backwarming from the chromosphere, which has been found in simulations (Allred et al. 2005; Allred et al. 2006; Cheng et al. 2010). As a consequence of the very disturbed and unknown state of the flaring atmosphere, the exact processes at play remain unidentified and it is possible that an unknown mechanism produces a flare spectrum that looks similar to a blackbody spectrum near 9000 K. As supported by our results and the other findings cited above and to compute the flare continuum energy, we assume in the following that the WL continuum follows a blackbody spectrum, thus keeping in mind that its origin is unclear, but that it is supported by various observations.

Assuming that the flare signal in the blue and green channels comes from blackbody radiation, we can make simple estimates; we first concentrate on the "average" M2 flare shown in Fig. 4. The ratio I_{blue}/I_{green} leads to a blackbody temperature of $T \sim 8941$ K (see Table 1). Multiplying the corresponding blackbody spectrum by the SPM blue channel response and matching the observed value at peak time, we obtain a flaring area on the solar surface of 2.8 arcsec^2. Integrating the blackbody spectrum with this flaring area leads to a total continuum emission at peak time of 6.2×10^{-3} W m^{-2}, i.e., about ~70% of the total radiated energy at peak time (9×10^{-3} W m^{-2} for the TSI). We stress here that the estimation of the total energy contained in the WL continuum is independent of the one deduced from the TSI observations. Doing the same exercise for the total energy radiated over time where the TSI flare profile is available, we find a mean flaring area of 1.4 arcsec^2 corresponding to a total continuum energy of 3.4×10^{30} erg to be compared with the observed total 5.2×10^{30} erg, i.e. 60%. Six percent comes from wavelengths

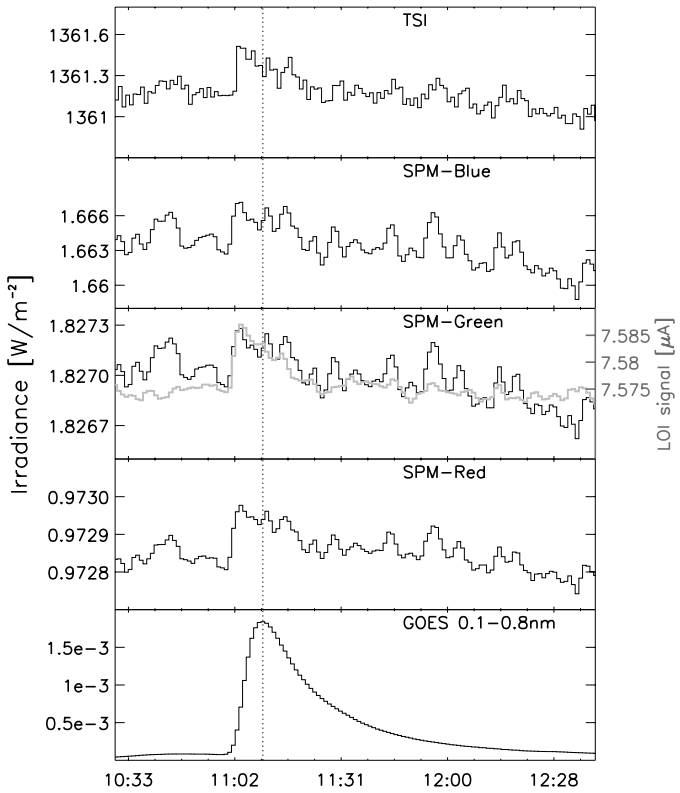


Fig. 6. Single flare light curves for the X17 flare of October 28, 2003. The grey curve in the third panel is the flux coming from a region of ~900 arcsec^2 that includes the flare site and was observed by the VIRGO/LOI instrument (Appourchaux et al. 1997) in the same passband as SPM/Green. SEM and GOES 0.01–0.5 nm are not shown because they are polluted by saturation and particle effects.

below 50 nm; the remaining could come from EUV wavelengths above 50 nm and from the visible and near UV emission of chromospheric origin as well as from H free-bound continuum. We did this exercise for all five sets of flares and present the deduced parameters of the blackbody radiation in Table 1. The contribution of the WL continuum is similar in all cases, i.e., around 70%. The estimated flaring areas are consistent with WLF observations (e.g. Hudson et al. 2006) and increase with the flare magnitude. Finally let us also note that other emission mechanisms with similar spectral distribution should lead to similar estimates of the flare energy contained in the white-light and near UV continuum.

4.2. The case of the X17 flare on October 28, 2003

The X17 flare that occurred on October 28, 2003 is a very large flare and the only one that has been unambiguously detected in TSI (Woods et al. 2004). Figure 6 shows irradiance light curves for this flare and confirms this finding by showing the flare signature in the SOHO/VIRGO instrument, while Woods et al. used the TIM instrument onboard SORCE. The increase in VIRGO is 264 ppm while it is 268 ppm in the TIM measurements, i.e., they agree very well. It also shows for the first time a clear white-light signature in Sun-as-a-star observations of a single flare using the VIRGO/SPM channels (relative increase of 267 ppm, 191 ppm, and 176 ppm for the blue, green, and red channel respectively). Note that the visible light and TSI peak about 5 min before SXR, confirming the importance of the impulsive phase.

Following the analysis of the previous section, we find that the ratio $I_{\rm blue}/I_{\rm green}$ is 1.28, which corresponds to a blackbody temperature of 8545 K, comparatively lower than in the average cases of the previous sections, although still consistent. The signal-to-noise ratio is lower in this single event than in the average cases but this somehow gives an idea of the uncertainty on the determination of the blackbody temperature and we should speak of a temperature *roughly around* 9000 K, that does not change very much with the amplitude of the flare. Matching the observed blue signal gives a flaring area of ~130 arcsec^2; this is much larger than areas shown in Table 1, but it should not be surprising for such a flare; it also agrees with white-light observations from the global oscillation network group (GONG) – see Figs. 4 and 7 of Maurya & Ambastha (2009). Integrating then a blackbody spectrum at 8545 K over this flaring area, we find that the blackbody spectrum accounts for 64% of the total energy, which agrees well with what we found for the average cases in Table 1.

5. Conclusions

We identified and analyzed for the first time the visible light produced by flares in Sun-as-a-star observations. We use a superposed epoch analysis to show that visible emission is present on average for all flares from X-ray class X to C, that it occurs mainly during the impulsive phase and must be considered as continuum emission, i.e., white-light flares. Analysing the intensity ratio of the SPM blue and green channels, we found this emission to be consistent with a blackbody spectrum near 9000 K. We then matched the increase observed in the blue channel and deduced flaring areas that are consistent with previous observations. Using these results, we computed the total energy contained in the continuum and found it to represent about 70% of the total energy radiated by flares. This study shows that the white light continuum is ubiquitous in flares and that it represents about two thirds of the energy radiated by the flares. Furthermore, we revealed the existence of white light signature in total solar flux for the single X17 flare that occurred on October 28, 2003 and find similar energy distribution.

These results show the very large predominance of the lower atmosphere with respect to the corona in freeing the flare energy that is initially stored in the solar magnetic field, and put constraints on models. Additionally, because each flare releases most of its energy in white light and there is a continuum of flares, we can wonder if the visible emission released by flares can contribute to the variations of the TSI. We plan to address these questions in a forthcoming study.

Acknowledgements. This work has received funding from the European Community's Seventh Framework Programme (FP7/2007-2013) under the grant agreement No. 218816 (SOTERIA project, www.soteria-space.eu). The author thanks T. Appourchaux for the VIRGO/LOI data, C. Wehrli for providing the SPM response functions, T. Dudok de Wit for useful discussions, and an anonymous referee for useful comments and suggestions.

References

Allende Prieto, C., & Garcia Lopez, R. J. 1998, A&AS, 131, 431
Allred, J. C., Hawley, S. L., Abbett, W. P., & Carlsson, M. 2005, ApJ, 630, 573
Allred, J. C., Hawley, S. L., Abbett, W. P., & Carlsson, M. 2006, ApJ, 644, 484
Appourchaux, T., Andersen, B. N., Frohlich, C., et al. 1997, Sol. Phys., 170, 27
Canfield, R. C., Penn, M. J., Wulser, J., & Kiplinger, A. L. 1990, ApJ, 363, 318
Carrington, R. C. 1859, MNRAS, 20, 13

Cessateur, G., Kretzschmar, M., Dudok de Wit, T., & Boumier, P. 2010, Sol. Phys., 263, 153
Chance, K., & Kurucz, R. L. 2010, J. Quant. Spectr. Rad. Trans., 111, 1289
Cheng, J. X., Ding, M. D., & Carlsson, M. 2010, ApJ, 711, 185
Falchi, A., Falciani, R., & Smaldone, L. A. 1992, A&A, 256, 255
Fletcher, L., Hannah, I. G., Hudson, H. S., & Metcalf, T. R. 2007, ApJ, 656, 1187
Hale, G. E. 1931, ApJ, 73, 379
Hawley, S. L., Allred, J. C., Johns-Krull, C. M., et al. 2003, ApJ, 597, 535
Heinzel, P., Karlicky, M., Kotrc, P., & Svestka, Z. 1994, Sol. Phys., 152, 393
Hudson, H. S., Wolfson, C. J., & Metcalf, T. R. 2006, Sol. Phys., 234, 79
Jess, D. B., Mathioudakis, M., Crockett, P. J., & Keenan, F. P. 2008, ApJ, 688, L119
Jiménez, A., Jiménez-Reyes, S. J., & García, R. A. 2005, ApJ, 623, 1215
Judge, D. L., McMullin, D. R., Ogawa, H. S., et al. 1998, Sol. Phys., 177, 161
Kowalski, A. F., Hawley, S. L., Holtzman, J. A., Wisniewski, J. P., & Hilton, E. J. 2010, ApJ, 714, L98
Kretzschmar, M., Dudok de Wit, T. D., Schmutz, W., et al. 2010, Nature Phys., 6, 690
Matthews, S. A., van Driel-Gesztelyi, L., Hudson, H. S., & Nitta, N. V. 2003, A&A, 409, 1107
Maurya, R. A., & Ambastha, A. 2009, Sol. Phys., 258, 31
Neidig, D. F. 1989, Sol. Phys., 121, 261
Schmieder, B., Fang, C., & Harra-Murnion, L. K. 1998, Sol. Phys., 182, 447
Švestka, Z. 1966, Space Sci. Rev., 5, 388
Thuillier, G., Floyd, L., Woods, T. N., et al. 2004, Adv. Space Res., 34, 256
Wang, H.-M. 2009, Res. Astron. Astrophys., 9, 127
Woods, T. N., Eparvier, F. G., Fontenla, J., et al. 2004, Geophys. Res. Lett., 31, 10802
Woods, T. N., Kopp, G., & Chamberlin, P. C. 2006, J. Geophys. Res., 111, A10S14